Author/s:
Yu, H;Palazzolo, JS;Ju, Y;Niego, B;Pan, S;Hagemeyer, CE;Caruso, F

Title:
Polyphenol-Functionalized Cubosomes as Thrombolytic Drug Carriers

Date:
2022-11-02

Citation:
Yu, H., Palazzolo, J. S., Ju, Y., Niego, B., Pan, S., Hagemeyer, C. E. & Caruso, F. (2022). Polyphenol-Functionalized Cubosomes as Thrombolytic Drug Carriers. Advanced Healthcare Materials, 11 (21), https://doi.org/10.1002/adhm.202201151.

Persistent Link:
https://hdl.handle.net/11343/315740

Polyphenol-Functionalized Cubosomes as Thrombolytic Drug Carriers

Haitao Yu, Jason S. Palazzolo, Yi Ju, Be'eri Niego, Shuaijun Pan, Christoph E. Hagemeyer, and Frank Caruso**

H. Yu, Y. Ju, S. Pan, F. Caruso
Department of Chemical Engineering, The University of Melbourne, Parkville, Victoria 3010, Australia
E-mail: fcaruso@unimelb.edu.au

J. S. Palazzolo, B. Niego, C. E. Hagemeyer
NanoBiotechnology Laboratory, Australian Centre for Blood Diseases, Central Clinical School, Monash University, Melbourne, Victoria 3004, Australia
E-mail: christoph.hagemeyer@monash.edu

Y. Ju
School of Health and Biomedical Sciences, RMIT University, Bundoora, Victoria 3083, Australia

Keywords: lipid cubosomes, metal–polyphenol networks, thrombolytic nanoparticles, plasminogen activators, urokinase

The safe administration of thrombolytic agents is a challenge for the treatment of acute thrombosis. Lipid-based nanoparticle drug delivery technologies present opportunities to overcome the existing clinical limitations and deliver thrombolytic therapy with enhanced therapeutic outcomes and safety. Herein, lipid cubosomes as nanocarriers are used for encapsulating thrombolytic drugs is examined. The lipid cubosomes are coated with a low-fouling peptide that is incorporated within a metal–phenolic network (MPN) and which encapsulate the thrombolytic drug urokinase-type plasminogen activator (uPA). The peptide-containing MPN (pep-MPN) coating inhibits the direct contact of uPA with the surrounding environment, as assessed by an in vitro plasminogen activation assay and an ex vivo whole blood clot degradation assay. The pep-MPN-coated cubosomes prepared with 22 wt% peptide demonstrate a cell membrane-dependent thrombolytic activity, which is attributed to their fusogenic lipid behavior. Moreover, compared with the uncoated lipid cubosomes, the uPA-loaded pep-MPN-coated cubosomes demonstrate significantly reduced nonspecific cell

association (<10% of the uncoated cubosomes) in the whole blood assay, prolonged circulating half-life, and reduced splenic uPA accumulation in mice. These studies confirm the preserved bioactivity and cell membrane-dependent release of uPA within pep-MPN-coated lipid cubosomes, highlighting their potential as a delivery vehicle for thrombolytic drugs.

1. Introduction

The safe and effective delivery of therapeutic biomolecules is a major challenge toward achieving clinical translation of emerging drug delivery platforms, including nanoparticles (NPs). This is due to low site-specific accumulation, insufficient bioavailability and off-target effects that are often displayed by NPs.[1,2] Demands are therefore growing for the development of NP drug delivery systems that can overcome these limitations while offering improved therapeutic efficacy.

Lyotropic liquid crystals with a cubic phase (cubosomes) or hexagonal phase (hexasomes) have drawn significant interest because of their stability, high biocompatibility, high loading capacity, and sustained drug release properties.[3–5] As lipids are abundant in nature, lyotropic liquid crystalline cubic phases are ubiquitous in natural structures, such as cellular membranes, exoskeletons of beetles and weevils, butterfly wing scales and sea urchins.[6–9] Notably, the properties of cubosomes can also be beneficial for applications in the nanomedicine field. Cubosomes feature amphiphilic lipid bilayers that conform to infinite periodic minimal surfaces with relative structural stability,[10,11] allowing the encapsulation of hydrophobic, hydrophilic, and amphiphilic therapeutic components, such as small molecular drugs, peptides, nucleic acids, and proteins.[4,12–16] In addition, the lipid monoolein (MO) has desirable properties, such as minimal toxicity, high biodegradability, and biocompatibility.[17] With regard to their cellular interactions, lipid cubosomes, which are typically 150–300 nm in diameter, are considered too large for clathrin-mediated endocytosis and are therefore more likely to engage with the lipid bilayer of cells via membrane fusogenic mechanisms, leading to burst release of the encapsulated cargo. [4,18,19] Moreover, lipid cubosomes prepared with the inclusion of cationic lipids (e.g., dioleoyl-3-trimethylammonium propane (DOTAP)) show increased binding to the negatively charged cell membrane, thereby accelerating fusogenic cellular interactions.[18,20] However, the nonspecific fusogenic interactions between lipid cubosomes and cellular membranes in vivo limit the prospects of achieving targeted drug delivery and can lead to rapid blood clearance.

Of particular relevance to our work, cubosomes might offer benefits for the delivery of plasminogen activators (PAs) for thrombolytic therapy. PAs are potent serine proteases that have been used as first-line treatments for thrombus dissolution in acute ischaemic events, like myocardial infarction and stroke. However, their use also faces several clinical limitations, including short half-life due to rapid clearance and fast neutralization by endogenous inhibitors, and a restricted therapeutic window owing to serious side effects, mainly bleeding. The latter is particularly associated with the second-generation, non-fibrin-dependent urokinase-type plasminogen activator (uPA).[21,22] Notably, several of the cubosomal properties specified above (including their cargo versatility, high loading capacity, biocompatibility, and burst release mechanism) could render cubosomes superior for PA delivery in comparison to alternative NP technologies, such as magnetic NPs,[23] electrostatically charged NPs,[24] and lipid vesicles.[25] Recently, we demonstrated the assembly of tannic acid–uPA-based NPs through template-assisted assembly.[26] Although these particles could load and release active uPA, in the context of emergency thrombolysis, an almost instantaneous release of the thrombolytic cargo is needed to achieve the efficacious drug dose for rapid reperfusion of brain tissue, before the brain is permanently damaged. This key requirement might be achieved by using cubosomes that exhibit a high loading capacity and burst release of active cargo, attributed to the high specific surface area of the cubosomes and membrane fusion mechanism. However, to prevent the nonspecific burst release of drug cargo from PA-loaded cubosomes, which may considerably increase the risk of severe side effects, like hemorrhagic complications,[27] in the current work, we coat the lipid cubosomes encasing the thrombolytic drug with metal–phenolic networks (MPNs) to form a shielded drug nanocarrier system. MPNs are known to form robust coatings on a range of substrates.[28–31] Taken together, the use of coated cubosomes to encapsulate, protect, and aid the delivery of biomacromolecular enzymatic drugs, such as PAs, may provide improved treatment efficacy in thrombolytic and other medical applications.

In the present study, we demonstrate (1) that lipid cubosomes can serve as nanocarriers for thrombolytic drugs and (2) the application of MPNs as coating to shield the uPA-encapsulating cubosomes from the surrounding environment. Specifically, gallic acid (GA) together with different amounts of a catechol-functionalized peptide (Pep-Cate) were used as the polyphenol to form the peptide-containing MPN (pep-MPN) coating. uPA activities were effectively inhibited in most pep-MPN-coated samples. The pep-MPN-coated uPA-loaded

lipid cubosomes with 22 wt% Pep-Cate (based on the mass of MO) presented a cell membrane-dependent activity and a lower plasminogen activation rate in the absence of cellular membranes. Yet, a higher clot busting activity was observed in an ex vivo cell-containing whole blood clot lysis assay, a result that is attributed to the fusogenic lipid behavior displayed by cubosomes. In addition, the pep-MPN-coated uPA-loaded lipid cubosomes displayed reduced nonspecific cell association in a whole blood assay and prolonged in vivo circulation compared with the uPA-loaded, uncoated cubosomes. These engineered cubosomal nanocarriers represent an advanced drug delivery platform for macromolecule-based therapies, which may be harnessed for administration of thrombolytic agents.

2. Results and Discussions

2.1. Synthesis and Characterization of pep-MPN-Coated Lipid Cubosomes as a Thrombolytic Drug Carrier

2.1.1. uPA@$^{-}$Cub and uPA@$^{+}$Cub

MO lipid cubosomes without/with cationic lipid DOTAP were used to load thrombolytic protein drug U-FRAG (uPA with human albumin as excipient) to form uPA-loaded lipid cubosomes with a negative charge and a positive charge (i.e., uPA@$^{-}$Cub and uPA@$^{+}$Cub, respectively), as shown in **Scheme 1**a. The amphiphilic lipid bilayers (consisting of MO or MO/1%DOTAP) were separated by internalized aqueous channels, which facilitate the encapsulation of hydrophilic bioactive cargos (i.e., proteins) in cubosomes, namely proteocubosomes, via a "nanopockets" mechanism.[32–35] DOTAP (1 mol% relative to MO) is the optimal value to obtain positively charged cubosomes according to the reports therein.[18,20] Pluronic F127 was used as a stabilizing agent to impart colloidal stability. As shown in **Figure 1**a and **Table 1**, uPA@$^{-}$Cub featured a particle size of 271 ± 117 nm and a polydispersity index (PDI) of 0.16, whereas uPA@$^{+}$Cub featured a particle size of 222 ± 100 nm and a PDI of 0.17. The ζ-potential values of uPA@$^{-}$Cub and uPA@$^{+}$Cub were −21 and 19 mV, respectively. Using confocal microscopy, uPA@$^{+}$Cub could be detected (Figure S1) at excitation wavelength of 633 nm owing to the presence of the fluorescence-labeled uPA (uPA-AF647 (Alex Fluor 647)), thereby indicating the successful loading of uPA in the lipid cubosomes. Transmission electron microscopy (TEM) and cryo-TEM imaging showed that the uPA@$^{-}$Cub and uPA@$^{+}$Cub featured particle sizes of ~200 nm (Figure 1b–e), which agrees with those measured in solution by dynamic light scattering (DLS) (Figure 1a). For TEM imaging, as the cubosomes were cast and dried on grids during sample preparation, they

were generally spherical. An outer shell was typically observed on both uPA@$^{-}$Cub and uPA@$^{+}$Cub cubosomes; particularly, the uPA@$^{+}$Cub featured an outer shell thickness of ~50 nm. The observed outer shell might be due to the electrostatic adsorption of stabilizer F127 and protein molecules on the cubosomes during TEM sample preparation, and thus the outer shell is much thicker for the positively charged uPA@$^{+}$Cub. In contrast, under cryo-TEM imaging conditions, the (square) morphologies of the uPA@$^{-}$Cub and uPA@$^{+}$Cub were retained with some vesicles observed on the outer surface of the cubosomes.

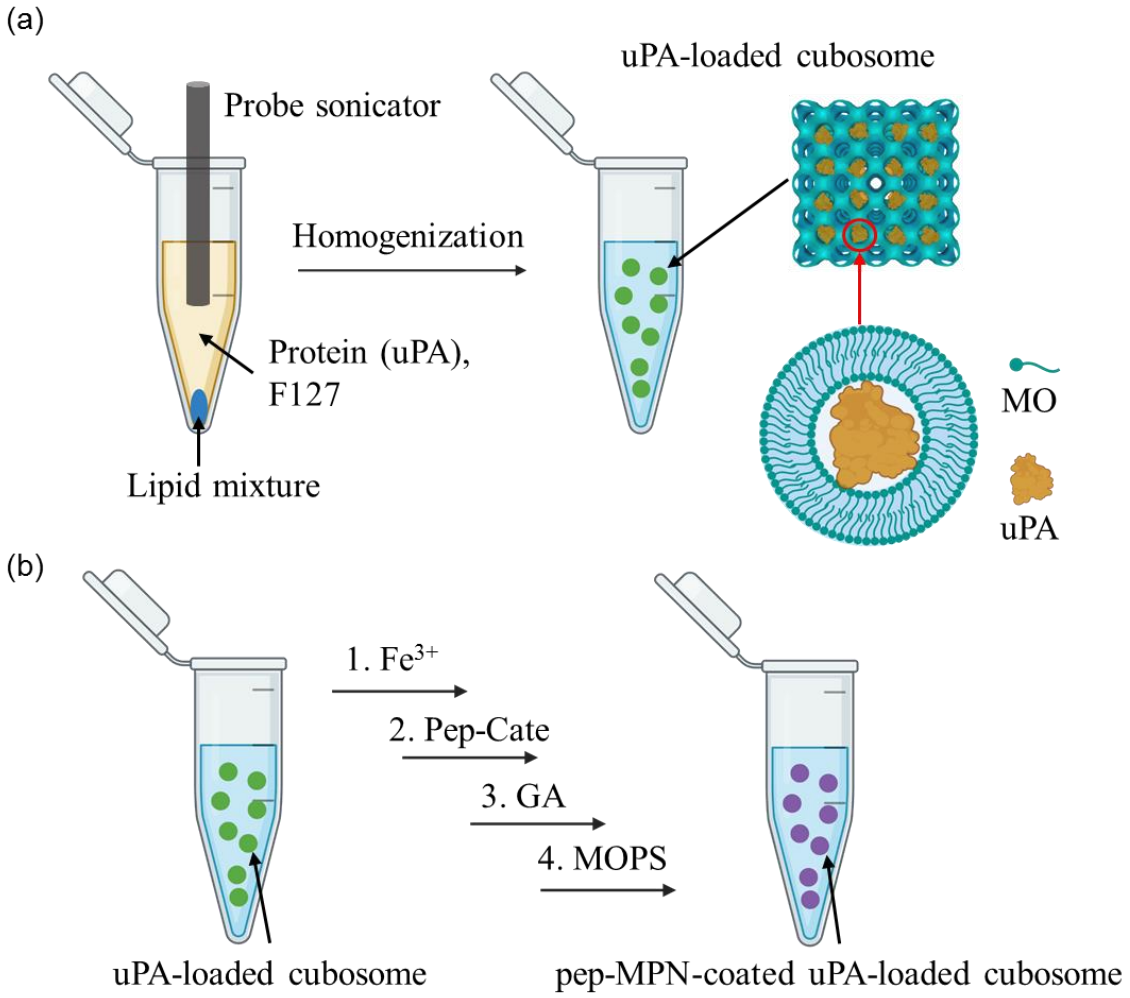

Scheme 1. (a) Preparation of protein drug (uPA)-loaded lipid cubosomes by homogenizing lipid mixture in the protein and F127 aqueous solution using probe sonicator. (b) Synthesis of pep-MPN-coated uPA-loaded cubosomes by sequentially adding different reagents (Fe^{3+} precursor, Pep-Cate, GA, 3-(N-morpholino)propanesulfonic acid (MOPS)) at the different steps.

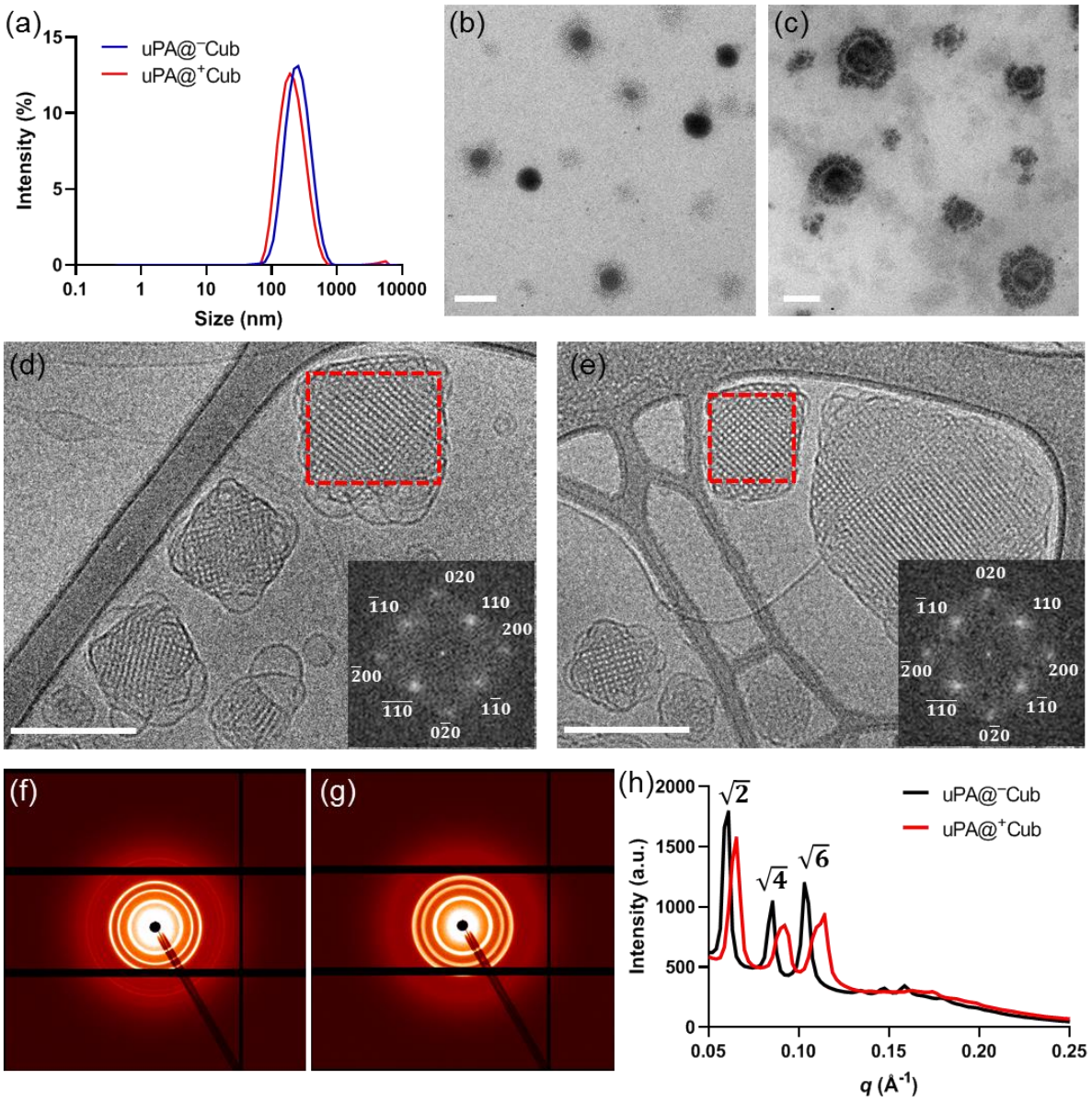

Figure 1. Characterization of uPA@⁻Cub and uPA@⁺Cub. (a) Size distribution profiles of the uPA-loaded lipid cubosomes obtained from DLS measurements. (b,c) TEM images and (d,e) cryo-TEM images with the corresponding FFT of the areas indicated by the red boxes (insets) of uPA@⁻Cub (b,d) and uPA@⁺Cub (c,e); scale bars: 200 nm. (f–h) 2D synchrotron SAXS scattering patterns of uPA@⁻Cub (f) and uPA@⁺Cub (g) and 1D synchrotron SAXS scattering patterns of the uPA-loaded lipid cubosomes.

The liquid crystalline structures of the uPA-loaded lipid cubosomes (uPA@⁻Cub and uPA@⁺Cub) were investigated using synchrotron small-angle X-ray scattering (SAXS). Both uPA@⁻Cub and uPA@⁺Cub showed a sequence of three well-defined diffraction peaks with relative positions at ratios of $\sqrt{2}$, $\sqrt{4}$, and $\sqrt{6}$, which corresponds to a primitive Im3m cubic structure with lattice parameters of ~145 and ~136 Å. These results suggest that the lipid cubosomes can load ~2 wt% macromolecular protein (based on the mass of MO) without destruction of the cubic phase nanostructure, as consistent with the phase identity of bovine

serum albumin (BSA)-loaded cubosomes reported therein.[15] The representative cryo-TEM images in Figure 1d,e also confirmed the presence of the ordered cubic phase pattern in uPA@$^{-}$Cub and uPA@$^{+}$Cub. In addition, the corresponding fast Fourier transform (FFT) patterns of the selected areas (defined by the red boxes) displayed the characteristic symmetry of Im3m cubic phase viewed along the [110] direction with a lattice parameter of ~160 Å, which agrees with the SAXS results.

Table 1. Particle size, PDI, and ζ-potential of the lipid cubosomes[a)]

Sample[b)]	Size [nm]	PDI	ζ-potential [mV]
uPA@$^{-}$Cub	271 ± 117	0.16	−21 ± 7
uPA@$^{+}$Cub	222 ± 100	0.17	19 ± 6
uPA@$^{-}$Cub@MPN	296 ± 157	0.17	−29 ± 7
uPA@$^{+}$Cub@MPN	209 ± 79	0.15	−28 ± 7
uPA@$^{+}$Cub@pep-MPN-1	233 ± 110	0.19	−15 ± 4
uPA@$^{+}$Cub@pep-MPN-2	231 ± 99	0.16	−15 ± 6
uPA@$^{+}$Cub@pep-MPN-3	235 ± 91	0.15	−17 ± 5

[a)]Data represent mean ± standard deviation (SD) of the average of three replicates for each sample.
[b)]The samples denote uncoated uPA-loaded lipid cubosomes, MPN-coated uPA-loaded lipid cubosomes (0 wt% Pep-Cate), and pep-MPN-coated uPA-loaded lipid cubosomes with varying amounts of Pep-Cate: 22, 44, and 110 wt% relative to the mass of GA (uPA@$^{-/+}$Cub, uPA@$^{-/+}$Cub@MPN, and uPA@$^{+}$Cub@pep-MPN-1–3 respectively)

2.1.2. uPA@$^{-}$Cub@MPN and uPA@$^{+}$Cub@MPN

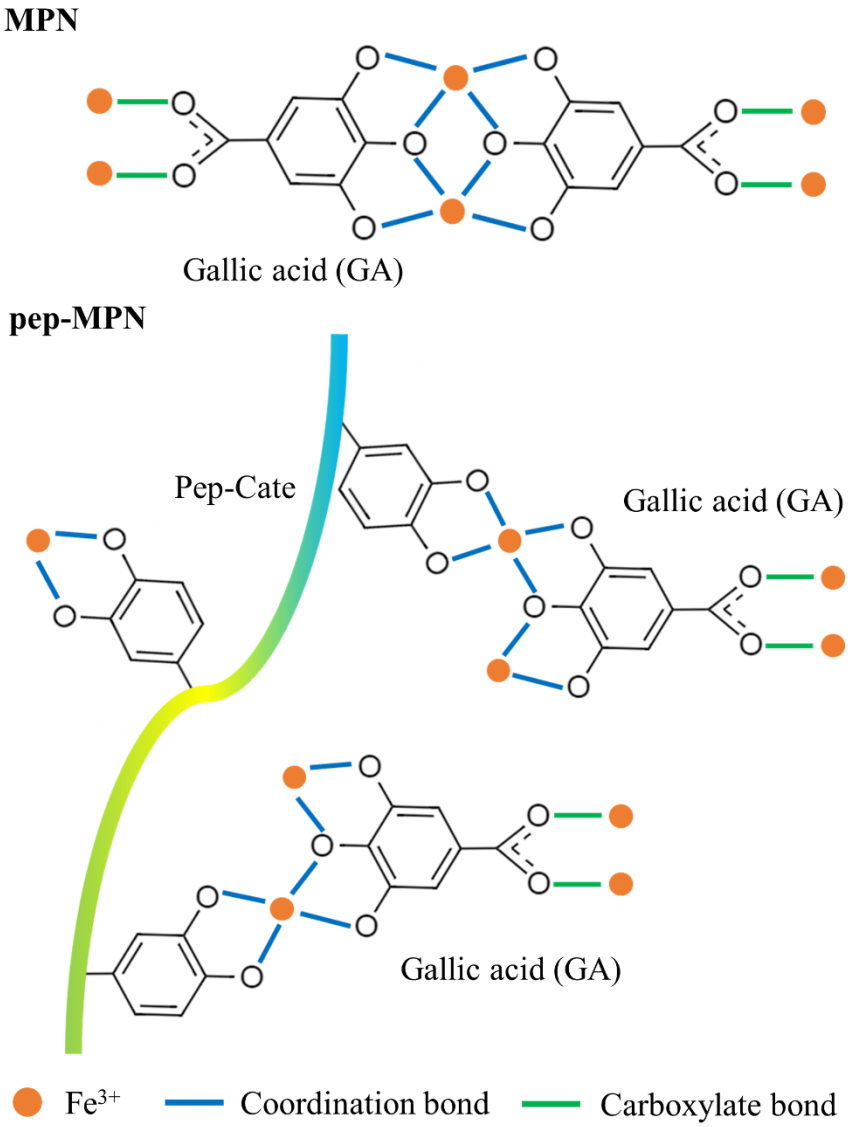

Scheme 2. Representative coordination modes in MPN and pep-MPN. Note that other coordination modes also exist in the system to form an integrated MPN or pep-MPN coating.

uPA-loaded lipid cubosomes (uPA@$^{-}$Cub and uPA@$^{+}$Cub) were coated with metal-coordinated phenolic ligands (GA as an example of a simple phenolic ligand) (in the presence of 0 wt% Pep-Cate) to produce uPA@$^{-}$Cub@MPN and uPA@$^{+}$Cub@MPN (see **Table 2**). The interactions between the cubosomes and MPNs are attributed to a combination of hydrogen bonding, metal coordination, and hydrophobic, electrostatic and π interactions. It has been reported that the carboxylic and hydroxyl groups of GA can provide sufficient binding sites for mono- and multinuclear Fe^{3+} species to form a large network via different coordination modes.[36,37] Representative coordination modes in MPN are displayed in **Scheme 2**, where the coordination bonds and carboxylate bonds in Fe^{3+}/GA MPN are drawn in blue and green, respectively. As observed from **Figure 2**a,b and Table 1, the formation of MPN on the uPA-loaded lipid cubosomes did not change the particle size but significantly

decreased the ζ-potential of both uPA@$^{-}$Cub and uPA@$^{+}$Cub to about –30 mV, indicating the successful coating of MPN on the uPA-loaded lipid cubosomes. The deposition of MPN on the uPA-loaded lipid cubosomes was also supported by the color (purple) of the uPA@$^{+}$Cub@MPN solution (Figure S2). TEM images (Figure 2c,d) of uPA@$^{-}$Cub@MPN and uPA@$^{+}$Cub@MPN show the spherical morphology of the cubosomes with a diameter of about 200 nm. In addition, a higher contrast was observed for uPA@$^{-}$Cub@MPN and uPA@$^{+}$Cub@MPN compared with that of uPA@$^{-}$Cub and uPA@$^{+}$Cub (Figure 1b,c). Energy-dispersive X-ray spectroscopy (EDX) elemental mapping of uPA@$^{+}$Cub@MPN (Figure 2e–h) revealed the presence of iron.

Table 2. Mass of reagents used for the syntheses of uPA@Cub@MPNs and uPA@Cub@pep-MPNs

Sample	MO [mg]	$FeCl_3 \cdot 6H_2O$ [µg]	Pep-Cate [µg]	GA [µg]
uPA@$^{-}$Cub@MPN	1	200	0	200
uPA@$^{+}$Cub@MPN	1	200	0	200
uPA@$^{+}$Cub@pep-MPN-1	1	200	44	200
uPA@$^{+}$Cub@pep-MPN-2	1	200	88	200
uPA@$^{+}$Cub@pep-MPN-3	1	200	220	200

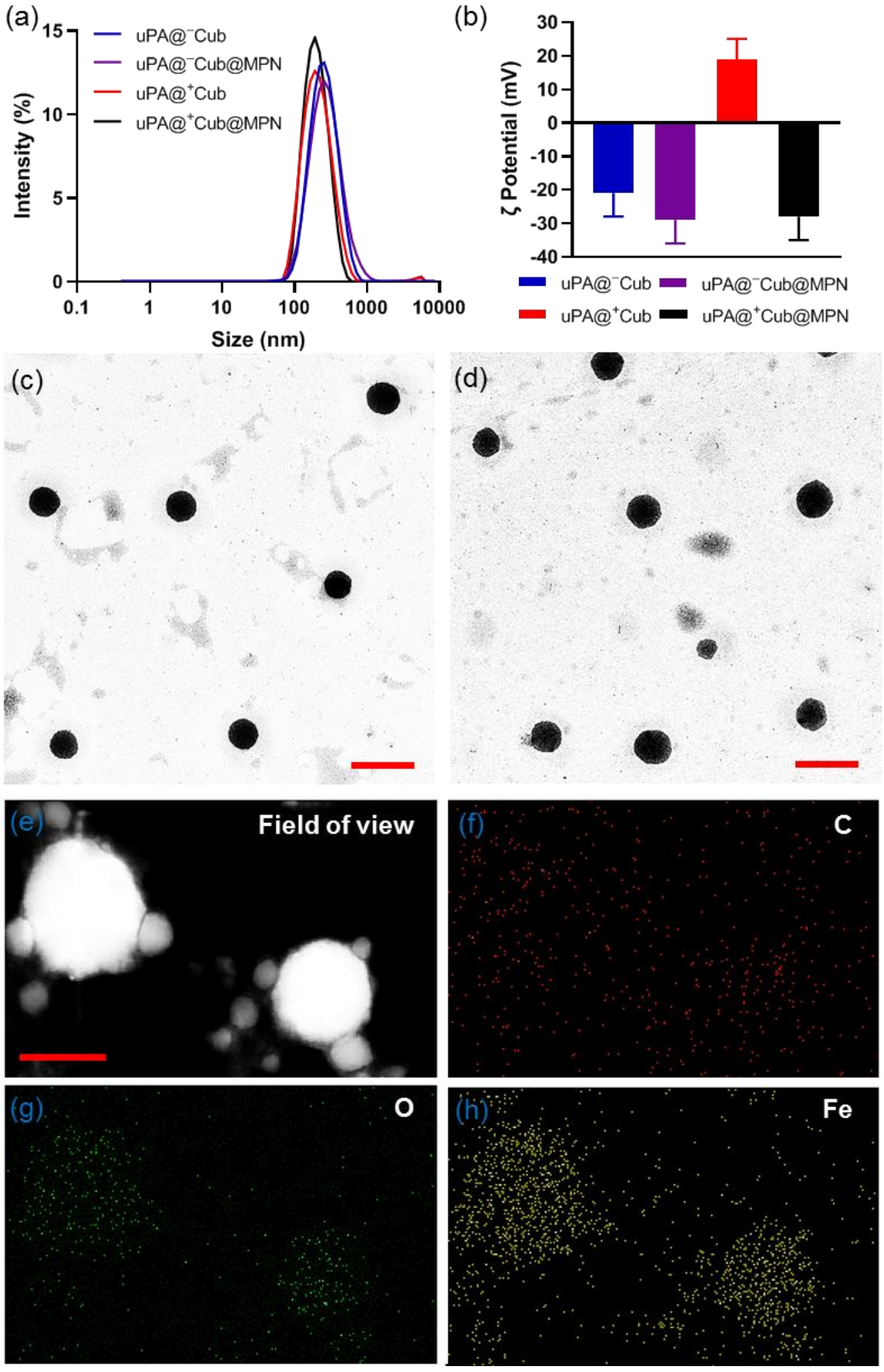

Figure 2. (a) Size distribution profiles (obtained from DLS measurements) and (b) ζ-potentials of the uPA@$^{-}$Cub, uPA@$^{+}$Cub, uPA@$^{-}$Cub@MPN, and uPA@$^{+}$Cub@MPN. In (b), data represent the mean ± SD (n = 3). (c,d) TEM images of uPA@$^{-}$Cub@MPN and uPA@$^{+}$Cub@MPN; scale bars are 500 nm. (e–h) EDX elemental mapping of uPA@$^{+}$Cub@MPN; scale bars are 200 nm.

2.1.3. uPA@$^{+}$Cub@pep-MPN-1–3

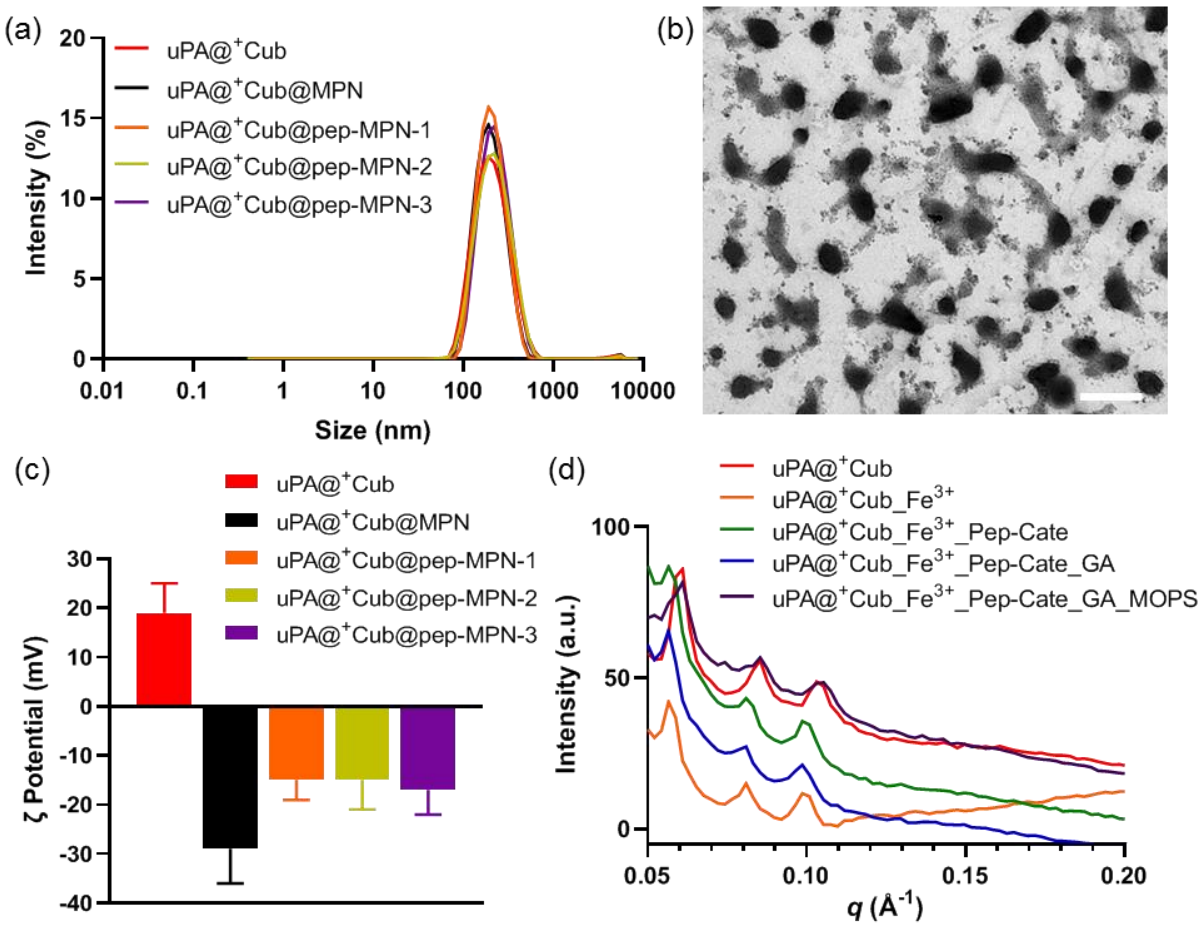

Figure 3. Characterization of pep-MPN-coated cubosomes. (a) Size distribution profiles (obtained from DLS measurements) of the uncoated and pep-MPN-coated uPA-loaded lipid cubosomes. (b) Representative TEM image of uPA@$^{+}$Cub@pep-MPN-2, scale bar is 200 nm. (c) ζ-potential of the uncoated and pep-MPN-coated uPA-loaded lipid cubosomes. The size distribution profile and ζ-potential of the uPA@$^{+}$Cub@MPN are shown from comparison. Data represent the mean ± SD (n = 3). (d) 1D Synchrotron SAXS scattering patterns of the products obtained after the sequential addition of different reagents (Fe^{3+} precursor, Pep-Cate, GA, MOPS) at the different steps during synthesis of the pep-MPN-coated cubosomes.

In addition to examining GA, a simple phenolic molecule, for preparing the MPN-coated uPA-coated cubosomes, a synthetic phenolic peptide (Pep-Cate), which was obtained by conjugating N-hydroxysuccinimide (NHS)-catechol groups and lysine in a proline–alanine–serine (PAS)-based peptide, was examined. The specific amounts of MO, $FeCl_3 \cdot 6H_2O$, Pep-Cate, and GA used during the synthesis of the different pep-MPN-coated cubosomes (uPA@$^{+}$Cub@pep-MPN-1–3) with varying Pep-Cate amounts, following Scheme 1b, are listed in Table 2. Representative coordination modes among Fe^{3+}, Pep-Cate, and GA in pep-MPN are displayed in Scheme 2. The formation of the pep-MPN-coated cubosomes is

indicated from the purple-colored solutions obtained (Figure S2). A lighter purple color was observed as more phenolic peptide was incorporated into the cubosomes.

Likewise, to the observations made on the size of the uPA@$^{+}$Cub@MPN cubosomes, the formation of uPA@$^{+}$Cub@pep-MPN-1–3 did not significantly change the particle size, with only a slight increase observed as more Pep-Cate was incorporated (**Figure 3**a and Table 1). TEM analysis of uPA@$^{+}$Cub@pep-MPN-2 revealed that the cubosomes had a diameter of ~200 nm and that the incorporation of Pep-Cate resulted in cubosomes with a less regular spherical morphology and the presence of debris in the background (Figure 3b). All peptide-incorporated samples (uPA@$^{+}$Cub@pep-MPN-1–3) featured a higher ζ-potential value between –10 and –17 mV compared with uPA@$^{+}$Cub@MPN (about –30 mV). Potential changes in the phase structure of the cubosomes at different stages during the synthesis of pep-MPN on uPA@$^{+}$Cub (i.e., uPA@$^{+}$Cub@pep-MPN-3) were monitored by synchrotron SAXS. The 1D synchrotron SAXS scattering patterns of the products obtained at the different stages in Figure 3d suggest that the primitive Im3m cubic structure was maintained throughout the synthesis.

uPA-AF647 was used to evaluate the loading of uPA in the samples. The fluorescence intensities of the samples were measured at an excitation wavelength of 620 nm; the samples featured a peak at 665 nm in the emission curves (Figure S3a). The loading amount of uPA-AF647 in individual cubosomes of the different samples was calculated as I/C_{NP}, where I represents the fluorescence intensity at 665 nm and C_{NP} is the concentration of the cubosomes (NPs μL^{-1}). As observed in Figure S3b, the I/C_{NP} values of the samples were comparable to each other, indicating a similar uPA loading amount in each cubosome. Therefore, C_{NP} was controlled to be consistent when comparing different samples in subsequent studies.

2.2. Thrombolytic Activity of uPA-Loaded Lipid Cubosomes

To assess the bioactivity of the therapeutic macromolecular cargo, the thrombolytic activity of the uPA-loaded lipid cubosomes was evaluated via a cell-free assay (in vitro plasminogen activation assay) and a cell-containing assay (ex vivo blood clot degradation assay).

2.2.1. In Vitro Plasminogen Activation (S-2251) Assay

The uPA-loaded lipid cubosomes were first examined in a cell-free system to measure any plasminogen activation activity in a passive diffusion manner. The absorbance profiles at 405

nm and the calculated plasminogen activation rates (PARs) (ΔA405 min^{-2}) of free uPA are plotted in **Figure 4**a,b. According to the standard curve shown as the inset in Figure 4b, the measured PARs correlated with uPA concentration. The cubosome samples were then examined alongside 10 nM free uPA (the equimolar equivalent of encapsulated uPA within the cubosomes). As observed in Figure 4c,d, a higher PAR was observed for uPA@$^{+}$Cub ($120 \times 10^{-4} \pm 2.5 \times 10^{-4}$ ΔA405 min^{-2}, $p < 0.0001$) compared with the control (10 nM free uPA, $76 \times 10^{-4} \pm 5.5 \times 10^{-4}$ ΔA405 min^{-2}). This suggests that uPA is either located in the internal aqueous channels or adsorbed on the surface of the lipid cubosomes and thus are in contact with the external aqueous environment. Concurrently, owing to possible multiple interactions among the components (plasminogen and S-2251 substrate) in the S-2251 assay, the cubosome matrix may work as a nanoreactor for the plasmin generation, consequently contributing to the enhanced PAR of uPA@$^{+}$Cub.

In contrast, the MPN- and pep-MPN-coated uPA-loaded lipid cubosomes showed significantly reduced PARs ($9.6 \times 10^{-7} \pm 4.5 \times 10^{-7}$, and $290 \times 10^{-7} \pm 7.5 \times 10^{-7}$, $233 \times 10^{-7} \pm 1.6 \times 10^{-7}$, and $2337 \times 10^{-7} \pm 41 \times 10^{-7}$ ΔA405 min^{-2}, respectively, for uPA@$^{+}$Cub@MPN, and uPA@$^{+}$Cub@pep-MPN-1–3) compared with 10 nM free uPA ($76 \times 10^{-4} \pm 5.5 \times 10^{-4}$ ΔA405 min^{-2}, $p < 0.0001$). These results reveal that the MPN (without Pep-Cate) and pep-MPN (with Pep-Cate) coating effectively encapsulate uPA within uPA@$^{+}$Cub (shielding uPA from the surrounding environment), and thus significantly reducing the plasminogen activity in the cell-free (S-2251) assay. The results obtained from this effective coating strategy is consistent with the previous observations made on Fe^{3+}/GA microcapsules with a thickness of ~7 nm that were almost nonpermeable (~0%) toward 70 kDa fluorescein isothiocyanate-dextran.[36] As the amount of Pep-Cate incorporated in the MPNs increased, the PAR increased. This trend is expected because of a less dense and more permeable pep-MPN in the presence of a large molecule (~7.4 kDa) and a relatively reduced amount of catechol groups per peptide molecule (maximum of 6 for single molecular), as displayed in Scheme 2.

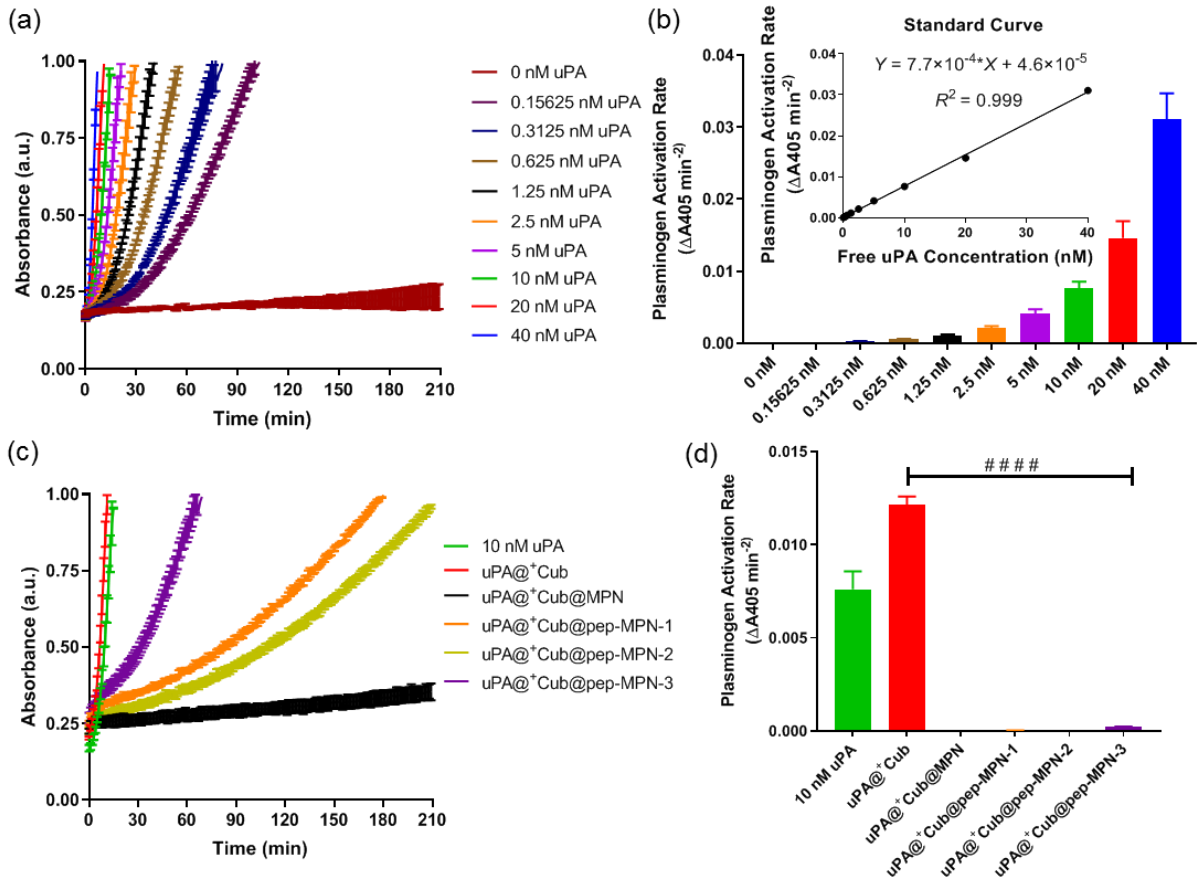

Figure 4. (a) Plasminogen activation assay absorbance curves at 405 nm of free uPA at varying concentrations ranging from 0 (blank) to 40 nM and (b) the corresponding fitted PARs and standard curve (inset). (c) Plasminogen activation rates of the cubosome samples at 1.6×10^{10} cubosomes mL^{-1} (equivalent to 10 nM uPA) and (d) the corresponding fitted PARs compared to 10 nM free uPA (from the standard curve). All data are presented as mean ± standard error of the mean (SEM) ($n = 3$); the data in (d) were analyzed by one-way ANOVA (no matching or pairing) with Dunnett's post-hoc test comparing each cubosome sample to 10 nM free uPA, $^{\#\#\#\#}p < 0.0001$.

2.2.2. Ex Vivo Blood (Halo) Clot Degradation Assay

To further confirm the effective encapsulation of uPA, an ex vivo blood clot degradation assay was conducted on the uPA-loaded lipid cubosomes. The assay results were analyzed according to the method described by Bonnard et al.[38] Using the absorbance values from the positive and negative controls, a "% clot degradation" curve was generated for each sample. Subsequently, the maximum clot lysis rate (CLR_{max}) was identified as the largest value of the slope calculated by performing a first-derivative analysis (no smoothing) of each curve. In **Figure 5**a,b, the percentage clot degradation profiles of free uPA showed a rightward shift with decreasing uPA concentration, corresponding to a slower clot degradation process.

As each cubosome sample was examined at 10 nM uPA equivalent (or 1.6×10^{10} cubosomes mL^{-1}), 10 nM uPA (free uPA) from the standard curve was chosen as a reference to compare the thrombolytic activity of the encapsulated uPA within each cubosome sample (Figure 5c,d). As observed in Figure 5d, uPA@$^{+}$Cub featured a CLR_{max} value comparable to that displayed by 10 nM free uPA (10.34 ± 2.23 min^{-1} and 7.92 ± 0.86 min^{-1}, respectively; p = 0.55). In contrast, the inclusion of an MPN coating (uPA@$^{+}$Cub@MPN) led to a significant reduction in CLR_{max} (0.95 ± 0.43 min^{-1} vs 7.92 ± 0.86 min^{-1} (10 nM uPA); p = 0.019). This significant reduction in CLR_{max} was maintained with the incorporation of 22 and 44 wt% Pep-Cate (relative to the mass of GA) in the pep-MPN coating of uPA@$^{+}$Cub@pep-MPN-1 and uPA@$^{+}$Cub@pep-MPN-2 (1.03 ± 0.11 min^{-1} and 0.79 ± 0.27 min^{-1}, respectively). The reduction in the CLR_{max} values of uPA@$^{+}$Cub@MPN and uPA@$^{+}$Cub@pep-MPN-1 and uPA@$^{+}$Cub@pep-MPN-2 is consistent with the results of the S-2251 assay, revealing that the pep-MPN coating with a relatively low Pep-Cate amount can efficiently encapsulate uPA.

In contrast, an increase in CLR_{max} (to 3.88 ± 1.58 min^{-1}) was observed for uPA@$^{+}$Cub@pep-MPN-3, which featured a higher amount (110% relative to the mass of GA) of Pep-Cate incorporated in the pep-MPN coating. The CLR_{max} value was comparable with that displayed by 5 nM free uPA (5.40 ± 1.00 min^{-1}). By comparison, the plasminogen activation of uPA@$^{+}$Cub@pep-MPN-3 corresponded to 0.24 nM free uPA in the S2251 cell-free assay. This significant (20-fold) enhancement of the thrombolytic activity displayed by uPA@$^{+}$Cub@pep-MPN-3 in the ex vivo environment is attributed to the membrane fusion process operating between the lipid cubosomes and cellular contents of the clots, which results in the release of uPA. Importantly, these results demonstrate that uPA@$^{+}$Cub@pep-MPN-3 can achieve high clot lysis activity, and also confirm that the bioactivity of uPA is preserved after being loaded within the pep-MPN-coated cubosome nanocarriers.

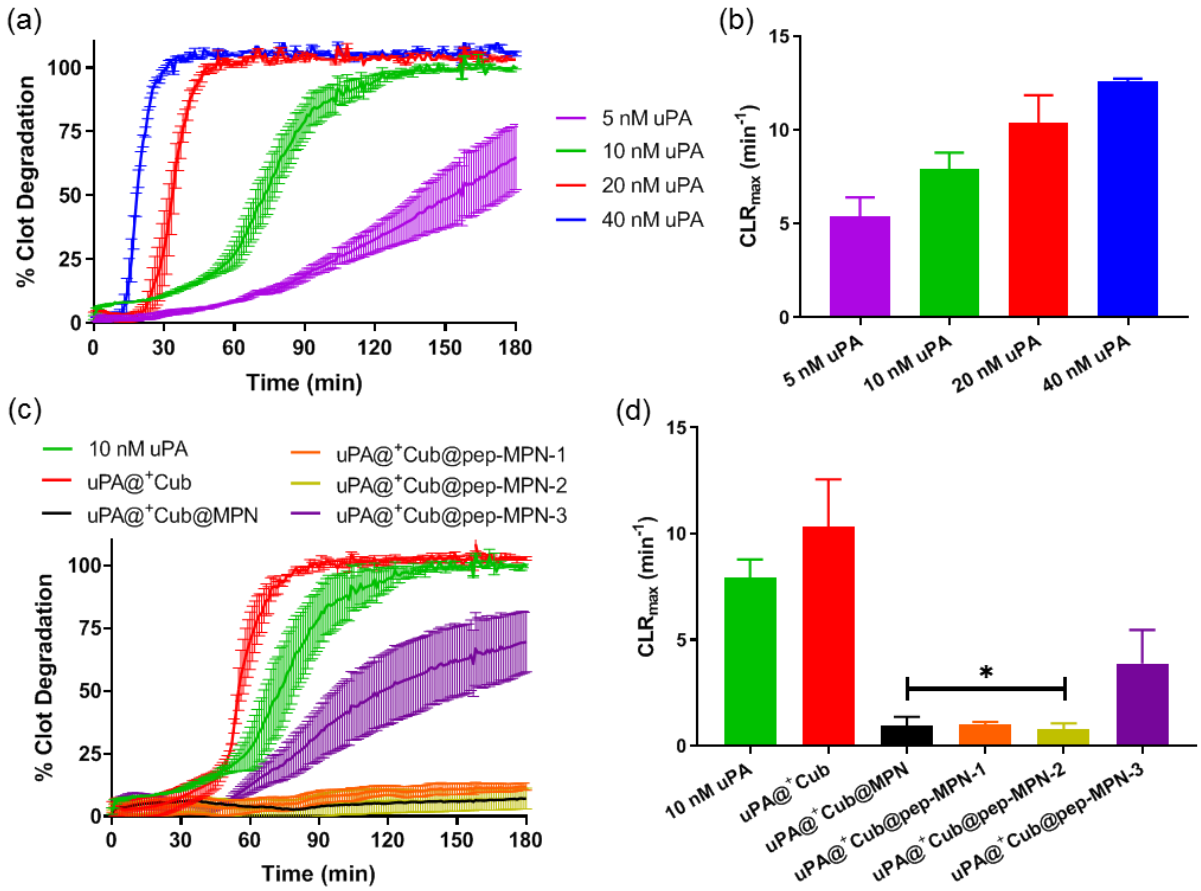

Figure 5. (a) Percentage clot degradation profiles of free uPA at different concentrations (5–40 nM) and (b) the corresponding CLR_{max} values calculated from the clot degradation curves. (c) Percentage clot degradation profiles of the cubosome samples at 1.6×10^{10} cubosomes mL^{-1} (equivalent to 10 nM uPA) and (d) the corresponding CLR_{max} values calculated from the clot degradation curves; the CLR_{max} of 10 nM free uPA (calculated from the standard curve) is also shown as a reference point. In (a–c), the data were subjected to first-derivative analysis (no smoothing), with the largest output value from each curve analyzed presented in (b) and (d) as the CLR_{max}. All data are presented as the mean ± SEM (n = 3). The data in (d) were analyzed by one-way ANOVA (paired) with Dunnett's post-hoc test comparing each cubosome sample to 10 nM uPA, *$p < 0.05$.

2.3. Biological Behavior of the uPA-Loaded Lipid Cubosomes

2.3.1. Immune Cell Association in Human Whole Blood

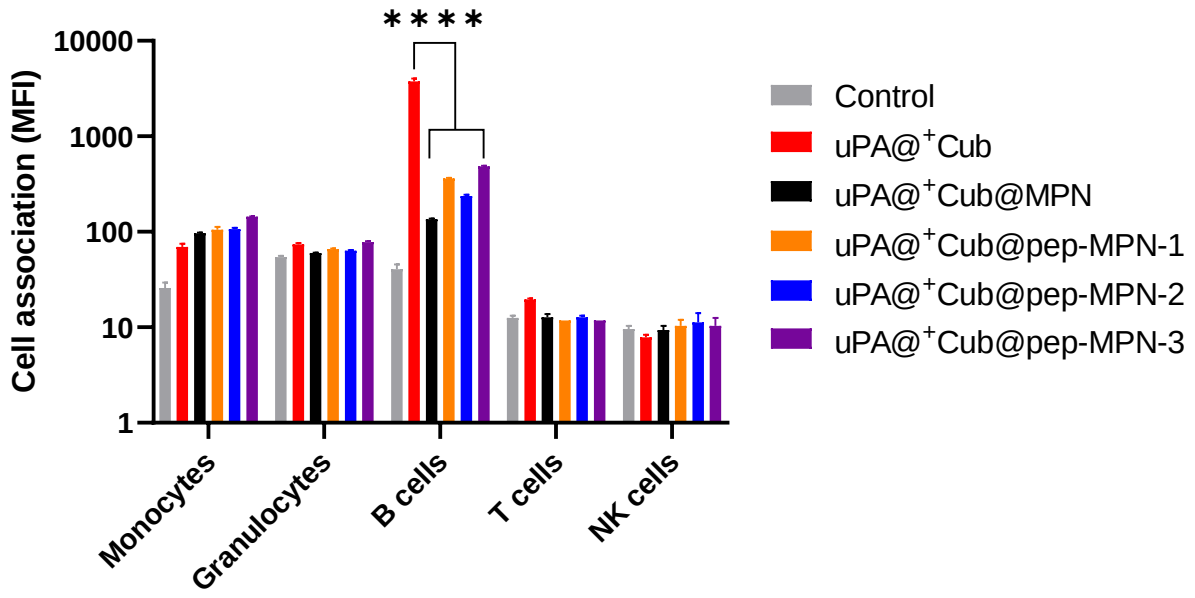

Figure 6. Association (measured as mean fluorescence intensity (MFI)) of uPA@$^{+}$Cub, uPA@$^{+}$Cub@MPN, and uPA@$^{+}$Cub@pep-MPN-1–3 with immune cells after incubation of the cubosomes for 1 h at 37 °C and a nanoparticle-to-cell ratio of 200:1 in whole human blood. Control refers to cell only samples. The data are presented as the mean ± SEM (n = 3) and analyzed by one-way ANOVA (no matching or pairing) with Dunnett's post-hoc test comparing each cubosome sample to uPA@$^{+}$Cub, ****$p < 0.0001$.

The bio–nano interactions of the uPA-loaded lipid cubosomes were assessed by performing a human whole blood assay to investigate particle association with human immune cells ex vivo. Fluorescent lipid DOPC-Cy5 was preloaded in the cubosome samples (i.e., uPA@$^{+}$Cub, uPA@$^{+}$Cub@MPN, and uPA@$^{+}$Cub@pep-MPN-1–3) to track the lipid matrix. Association of the cubosomes with monocytes, granulocytes, B cells, T cells, and NK cells was then determined using flow cytometry after incubation of the cubosomes in human whole blood for 1 h at 37 °C. As observed from **Figure 6**, uPA@$^{+}$Cub displayed a significantly higher association with B cells than with other cells; this is likely mediated by complement receptors on B cells as we previously observed on other polymer NPs.[39–41] When compared with the association behavior displayed by uPA@$^{+}$Cub with B cells, uPA@$^{+}$Cub@MPN and uPA@$^{+}$Cub@pep-MPN-1–3 displayed reduced immune cell association ($p < 0.0001$), which is likely due to the negative surface charge and the reduced membrane fusion behavior as a result of the coating, which inhibited direct contact between the cell membrane and lipid matrix. Comparison of the coated cubosomes revealed that uPA@$^{+}$Cub@pep-MPN-1–3 demonstrated a higher association (with B cells) than the uPA@$^{+}$Cub@MPN, which suggests that the pep-MPN coating containing (increasing amounts of) Pep-Cate may be more permeable than the coating without Pep-Cate. The cell association results agree with the

plasminogen activation data of the uPA-loaded lipid cubosomes obtained from the halo clot degradation assay (Figure 5c,d), thus revealing that a higher cell association (i.e., stronger membrane fusion) of the cubosomes contributes to a higher plasminogen activation of the uPA cargo.

2.3.2. In Vivo Biodistribution and Blood Clearance Studies

Considering the high risk of hemorrhagic complications of uPA, we only focused on the biological behavior of uPA@$^{+}$Cub@pep-MPN-2 because of its attenuated nonspecific activity of uPA determined in the ex vivo blood (halo) clot degradation assay and low-fouling Pep-Cate. Instead of tracking the lipid matrix as performed in the in vitro cell association, cyanide7.5 (Cy7.5)-labeled uPA (with human albumin as excipient) was used to study how the cubosome nanocarriers influenced the pharmacokinetics of the encapsulated protein drug. Detection of fluorescence from blood samples collected at designated time points post-injection, as well as selected organs/tissues collected at the experimental endpoint (60 min post-injection), revealed the influence of the cubosome nanocarriers on the pharmacokinetics of the encapsulated uPA (i.e., U-FRAG) relative to nonencapsulated (or free) uPA when administered at equivalent dosages.

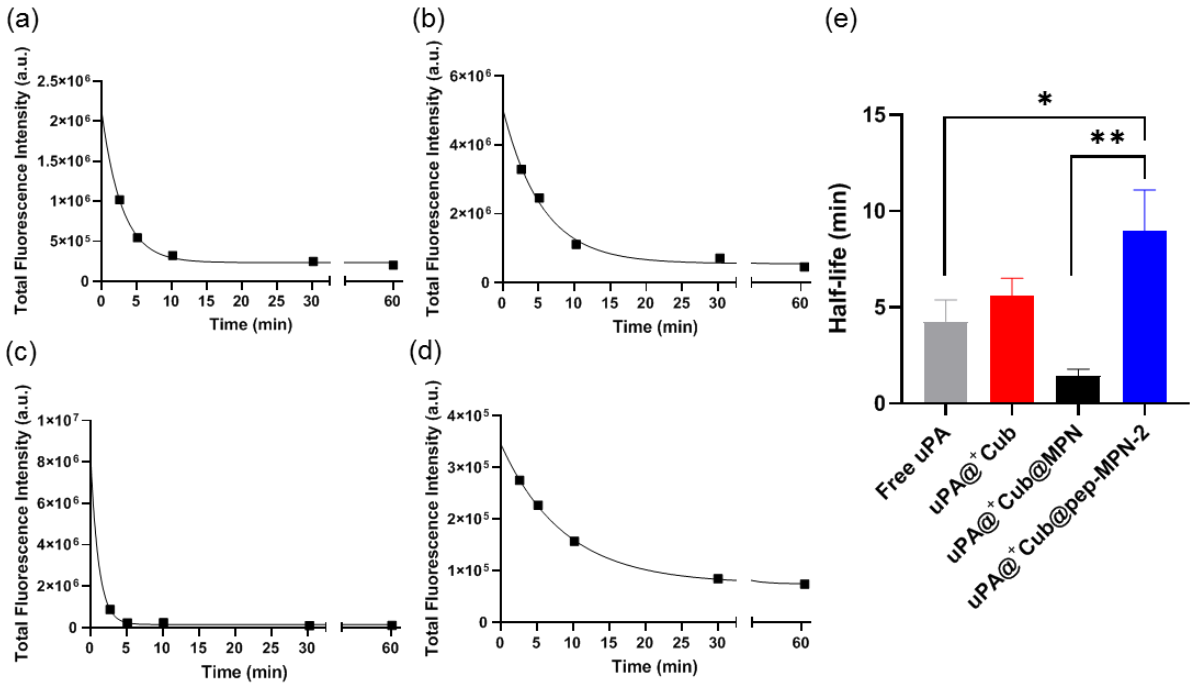

Figure 7. (a–d) Representative blood clearance profiles of Cy7.5-labeled uPA (free (a) and encapsulated within uPA@$^{+}$Cub (b), uPA@$^{+}$Cub@MPN (c), or uPA@$^{+}$Cub@pep-MPN-2 (d)) fitted to one-phase exponential decay and (e) the corresponding circulating half-life profiles of the Cy7.5-labeled uPA calculated from the blood clearance profiles. All data are presented as the mean ± SEM (n = 3) and analyzed by one-way ANOVA with uncorrected Fisher's least significant difference post-hoc test, *p < 0.05, **p < 0.01.

Figure 7a–d and Figure 7e show the blood clearance profiles and corresponding circulating half-life profiles of Cy7.5-labeled uPA (free and encapsulated within uPA@$^{+}$Cub, uPA@$^{+}$Cub@MPN, or uPA@$^{+}$Cub@pep-MPN-2). As observed from Figure 7e, uPA encapsulated within uPA@$^{+}$Cub or uPA@$^{+}$Cub@MPN showed no significantly different circulating half-lives (5.59 ± 0.91 min and 1.40 ± 0.38 min, respectively) to that of free uPA (4.26 ± 1.12 min; p = 0.49 and 0.16, respectively). In contrast, uPA encapsulated within uPA@$^{+}$Cub@pep-MPN-2 achieved a significantly prolonged circulating half-life (8.94 ± 2.16 min) compared to free uPA (p = 0.035) or uPA@$^{+}$Cub@MPN (p = 0.0036). This result reveals that the incorporation of an MPN with a synthetic low-fouling Pep-Cate can achieve prolonged circulation compared to an uncoated protein drug.

Likewise, the biodistribution of Cy7.5-labeled uPA (**Figure 8**) was influenced by whether it was encapsulated within the cubosome nanocarriers or nonencapsulated. Free uPA accumulated at similar levels in both the liver and spleen (p = 0.90), whereas the encapsulated uPA accumulated to a significantly larger extent in the liver than in the spleen, irrespective of the encapsulating cubosome type (uPA@$^{+}$Cub, p <0.0001; uPA@$^{+}$Cub@MPN, p = 0.0027; uPA@$^{+}$Cub@pep-MPN-2, p < 0.0001). Negligible levels of uPA accumulation were observed in the remaining organs (kidney, lung, heart, skeletal muscle, and brain) regardless of the encapsulated or nonencapsulated form of the systemically administered uPA.

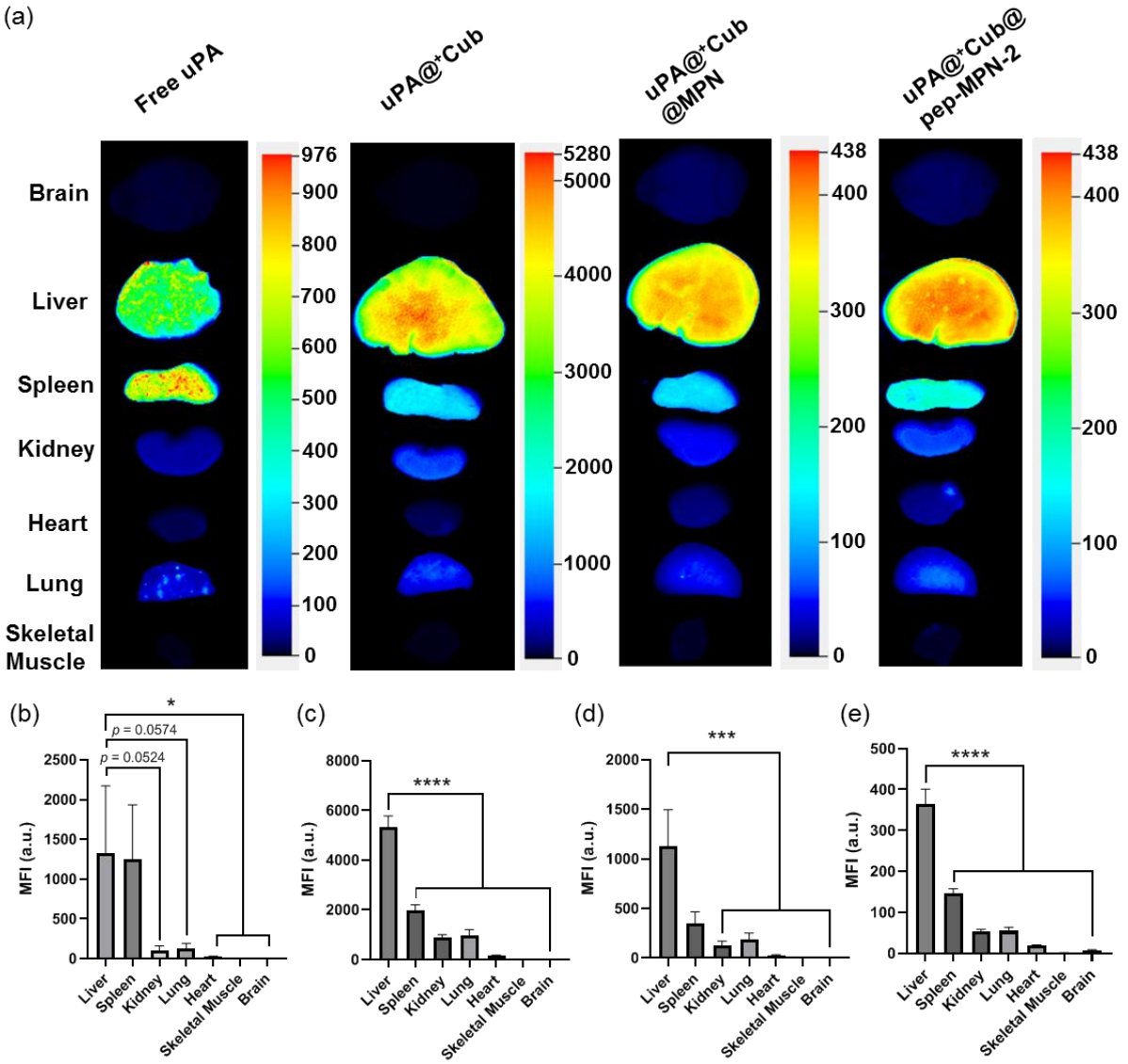

Figure 8. (a) Representative biodistribution scans of Cy7.5-labeled uPA in organs/tissues (brain, liver, spleen, kidney, heart, lung, and skeletal muscle) when administered as free uPA or within a nanocarrier (i.e., uPA@$^{+}$Cub, uPA@$^{+}$Cub@MPN, and uPA@$^{+}$Cub@pep-MPN-2). (b–e) Corresponding biodistribution analysis of Cy7.5-labeled uPA accumulation across various organs/tissues. All data are presented as the mean ± SEM (n = 3) and analyzed by one-way ANOVA with uncorrected Fisher's least significant difference post-hoc test, *p < 0.05, **p < 0.01, ****p < 0.0001.

3. Conclusions

In this work, we demonstrated the potential of lipid-based cubosomes to function as effective nanocarriers of thrombolytic drugs. The lipid cubosomes with ~2 wt% loading of macromolecular proteins (based on the mass of MO) had a size of ~200 nm and the primitive Im3m cubic phase nanostructure. These lipid-based, uPA-encapsulating cubosomes were subsequently coated with a pep-MPN without disrupting the size and phase of the lipid matrix. Moreover, from our in vitro plasminogen activation and ex vivo whole blood clot degradation assays, we conclude that the pep-MPN coating process not only preserved uPA

activity, but also effectively shielded uPA from the surrounding environment. This result implies that the premature release of the potent thrombolytic cargo was avoided, which has the potential to reduce the risk of adverse outcomes (such as hemorrhagic complications) in future in vivo work. Importantly, the uPA@$^{+}$Cub@pep-MPN-3 nanoparticle (that incorporated the highest amount of low-fouling Pep-Cate among all pep-MPN-coated samples examined) also demonstrated a cell-membrane dependent clot lysis activity ex vivo. This was inferred from low plasminogen activation rates in the absence of cell membrane structures (as shown by the S-2251 assay), but a robust enhancement (20-fold on the Halo assay) in degradation of whole blood clots that incorporate cellular elements. These observations are attributed to the fusogenic behavior of the lipid cubosomes with cell membranes. Furthermore, the pep-MPN-coated uPA-loaded lipid cubosomes showed reduced immune cell associations in human blood compared to their non-pep-MPN-coated counterparts. The biodistribution and blood clearance studies in mice (with uPA@$^{+}$Cub@pep-MPN-2) showed that the cubosomal pep-MPN coating influenced the pharmacokinetics of the encapsulated thrombolytic cargo, which displayed a prolonged circulating half-life and reduced splenic accumulation. The present study demonstrates the potential of engineered, polyphenol-functionalized lipid cubosomes to function as nanocarriers of thrombolytic drugs (and likely other macromolecule-based therapies for various medical conditions). Owing to their excellent biocompatibility, high loading capabilities and burst release of cargos during the membrane fusion process, pep-MPN-coated cubosomes may represent an innovative and feasible strategy to achieve an efficient clot lysis activity with low risk of bleeding complications for the treatment of acute cardiovascular events.

4. Experimental Section

Materials: Urokinase for injection (U-FRAG, lyophilized) was purchased from medac GmbH (Wedel, Schleswig-Holstein, Germany). MO, Pluronic® F-127, 4-(2-hydroxyethyl)-1-piperazineethanesulfonic acid (HEPES), anhydrous *N*,*N*-dimethylformamide (DMF), triethylamine (TEA), urea, Tween 20, NaCl, dimethyl sulfoxide (DMSO), 3-(N-morpholino)propanesulfonic acid (MOPS) buffer, and human glu-plasminogen were purchased from Sigma-Aldrich (St. Louis, MI, USA). Dulbecco's phosphate-buffered saline (DPBS), Alexa Fluor 647 succinimidyl ester (AF647 NHS ester), and Alexa Fluor 488 succinimidyl ester (AF488 NHS ester) were purchased from Life Technologies (Melbourne, Victoria, Australia). Cyanine7.5 NHS ester (Cy7.5 NHS) was purchased from Lumiprobe (Hunt Valley, MD, USA). 18:1 Cy5 PC (DOPC-Cy5) was purchased from Avanti Polar

Lipids Inc. (Alabaster, USA). Catechol-NHS and a low-fouling, custom-made peptide (H_2N-KGGPKAPAPS APAASPAAPS ELTPRGWRLE SAPAASPKAP KPASPAAPAA ELTPRGWRLE AASPAAPAPS KPAPASPAAK-COOH, molecular weight ~7.8 kDa) containing PAS and lysine (K) in the backbone were purchased from Shanghai Apeptide Co., Ltd. (Shanghai, China).

Synthesis of AF488-Labeled Pep-Cate: The amine groups of six lysines in the peptide were conjugated with Catechol-NHS and AF488 NHS via NHS chemistry, following a similar procedure to that previously reported for the synthesis of polyethylene glycol–polyphenol.[29,42] Briefly, the peptide (30 mg) was first dissolved in degassed DMF (700 µL) and mixed with AF488 NHS (170 µL, 1 mg mL^{-1} in DMSO, molar ratio of peptide/AF488 1:15). The mixture was stirred at room temperature for 1 h. Subsequently, catechol-NHS (30 mg, molar ratio of peptide/catechol 1:5) was then dissolved in degassed DMF (800 µL) and added to the above peptide/AF488 NHS mixture and stirred for 3 h. At last, 1 vol% TEA in DMF solution (5.5 µL, molar ratio of peptide/TEA 10:1) was added, and the mixture was stirred at room temperature overnight while protected from light. All procedures were performed under an argon atmosphere. After reaction, DMF was removed from the mixture via rotary evaporation. The resultant product was redissolved into Milli-Q water and purified by dialysis using a 3.5 kDa regenerated cellulose membrane (Thermo Fisher Scientific, USA) for 3 days against degassed acidic Milli-Q water (6 L, pH 3.5), and finally collected via lyophilization to obtain AF488-labeled Pep-Cate.

Preparation of uPA-Loaded Lipid Cubosomes: A lipid mixture was first prepared by mixing MO (50 mg) without/with 1% DOTAP (based on the mol% of MO) in ethanol and subsequent complete drying in a vacuum desiccator for several days. As shown in Scheme 1, the homogeneous lipid mixture was then homogenized by probe sonication (Branson ultrasonifier 250, 20% Duty Cycle, 3 s on/5 s off, 5 min) in an aqueous solution (1 mL) of F127 (5 mg mL^{-1}) and uPA (157 µg mL^{-1}, with 1 mg mL^{-1} human albumin as excipient), resulting in a stock solution of uPA-loaded lipid cubosomes, specifically, 5 wt% MO cubosomes with a negative or a positive charge (i.e., uPA@$^{-}$Cub and uPA@$^{+}$Cub). Cubosomes have been reported with a high protein loading capacity (e.g., 66.7 wt% relative to MO) without changing the cubic phase structure.[15] To obtain fluorescent cubosomes, DOPC-Cy5 (0.02 mg) was introduced at the lipid mixing stage. For the in vivo studies, Cy7.5-labeled uPA (human albumin as excipient) was used.

Synthesis of pep-MPN-Coated uPA-Loaded Cubosomes: The pep-MPN-coated uPA-loaded lipid cubosomes with varying amounts of Pep-Cate (uPA@$^{+}$Cub@pep-MPN-1–3, Table 2) were prepared according to a standard protocol as shown in Scheme 1. As an example, uPA@$^{+}$Cub@pep-MPN-1 was prepared by diluting uPA@$^{+}$Cub (20 µL) in water (458 µL) and mixing with $FeCl_3 \cdot 6H_2O$ solution (20 µL, 10 mg mL^{-1}) by vortexing (10 s). A Pep-Cate aqueous solution (22 µL, 2 mg mL^{-1}) was added, vortexed for 10 s, and incubated for 20 min. Then, a GA aqueous solution (20 µL, 10 mg mL^{-1}) was added to the mixture, vortexed for 10 s, and incubated for 20 min. Subsequently, 100 mM MOPS buffer (200 µL, pH 7.85) as the buffer solution[43] was added, followed by mixing via vortexing (10 s) and incubation for 20 min. The final solutions were purified using spinning desalting columns (dextran 7 kDa cutoff, Pierce/Thermo Scientific, IL, USA) and filtered with FilterBio® Nylon Syringe Filters (Nantong FilterBio Membrane Co., Ltd., Nantong, China) to remove the reagent residues (i.e., small pep-MPN complexes) and potential aggregations in bulk. For the different samples prepared, the specific masses of MO, $FeCl_3 \cdot 6H_2O$, Pep-Cate, and GA are listed in Table 2. The volume of the final solutions was the same (740 µL) across all samples by adjusting the volumes of water and peptide solution.

Characterization: TEM imaging of the cubosomes was performed on an FEI Tecnai Spirit TEM (FEI, OR, USA) at an operation voltage of 80 kV. High-angle annular dark-field imaging and EDX mapping were performed on a FEI Tecnai F20 TEM (FEI, OR, USA) operating at 200 kV. Confocal microscopy was performed on a Nikon A1R+ confocal laser scanning microscope (Nikon Corporation, Japan). To determine the size distribution of the cubosomes, DLS analysis was performed on a Zetasizer Nano ZS instrument (Malvern Instrument, Worcestershire, UK). The ζ-potentials of the cubosomes were determined on a Zetasizer Nano ZS instrument. Solutions of cubosomes were diluted 20× in water. The refractive indices of MO and water were 1.46 and 1.33, respectively. The fluorescence intensities of the samples were measured on a Fluorolog spectrofluorometer (Horiba Scientific, UK).

Fluorescence Pre-Labeling of uPA: Fluorescence pre-labeling of uPA was achieved via NHS chemistry between the amine residues in the protein and AF647 NHS or Cy7.5 NHS. Briefly, uPA (600 µL, 1.57 mg mL^{-1}) in Milli-Q water was mixed with AF647 NHS (20 µL, 1 mg mL^{-1} in DMSO) or Cy7.5 NHS (20 µL, 25 mg mL^{-1} in DMSO). The NHS reaction proceeded

at room temperature (22 °C) for 3 h with gentle incubation on a rotary wheel, followed by purification using a desalting spin column (dextran 7 kDa cutoff) to remove excess unreacted dye molecules. The reaction mixture was shielded from light throughout the process.

In Vitro Plasminogen Activation (S-2251) Assay: To measure the plasminogen activation potential of the cubosomes in the absence of cellular membranes, a cell-free assay was performed using the plasmin chromogenic substrate S-2251 (Chromogenix; Bedford, MA, USA). Reaction mixtures were prepared in the wells of a flat-bottom, transparent, nonpyrogenic, polystyrene, tissue culture-treated, sterile 96-well plate (Corning; ME, USA). Each reaction mixture contained S-2251 (25 µL, 0.5 mM), human plasminogen (25 µL, 0.5 µM; Sigma-Aldrich), and the reaction buffer (25 µL, 50 mM HCl with 0.01% Tween 80, pH 7.4). To each reaction mixture, the different cubosome samples (25 µL) were then added at an identical final concentration of 1.6×10^{10} cubosomes mL^{-1} (equivalent to 10 nM uPA). A standard curve using free uPA (U-FRAG) was tested alongside the cubosome samples. The standard curve concentrations were 0.00 (blank), 0.156, 0.313, 0.625, 1.25, 2.50, 5.00, 10.0, 20.0, 40.0 nM. Prior to reaction initiation, the reaction wells contained S-2251 and plasminogen only. The reaction was initiated once the uPA-containing samples (free uPA or uPA-loaded lipid cubosomes) were added to the reaction wells. The plate was then immediately placed into a FLUOstar Optima microplate reader (BMG Labtech; Victoria, Australia) set to 37 °C, and absorbance measurements were performed once every minute (10 flashes per read) for 3.5 h at 405 nm. All concentrations stated represent the final concentrations in the 100 µL reaction volume.

The raw absorbance values were then plotted and all absorbance values greater than 1.0 were excluded. Using GraphPad Prism, the remaining data were fitted to a second-order polynomial (quadratic) non-linear regression ($Y = A + BX + CX^2$). The resulting equation was twice differentiated ($2C$) to yield the PAR. The PAR standard curves were plotted at each respective uPA concentration and fitted to a linear regression ($Y = \alpha + \beta X$).

Ex Vivo Blood (Halo) Clot Degradation Assay: The experimental use of human blood was approved by the Monash University Human Research Ethics Committee (Project 67/15). Blood from healthy volunteers was collected using a 19-gauge butterfly needle into syringes containing 3.2% sodium citrate [blood/anticoagulant ratio = 9:1 (v/v)]. All volunteers signed

an informed consent form prior to blood collection and confirmed that no medications that could affect hemostasis were taken in the 10 days leading up to blood collection.

The assay was performed according to the methodology described in Bonnard et al.,[38] with minor variations described here. Clot formation was induced using a clotting mixture of 4 U mL^{-1} Human Thrombin (Human Plasma, High Activity; EMD Millipore, Burlington MA, USA) and 67 mM $CaCl_2$ prepared in HEPES buffer (25 mM HEPES, 137 mM NaCl, pH 7.4). "Halo-" shaped clots were produced on the bottom edge of the wells within a flat-bottom, transparent, nonpyrogenic, polystyrene, tissue culture-treated, sterile 96-well plate (Corning). A droplet of the clotting mixture was aliquoted (5 µL) onto the base of the well followed by the addition of blood (25 µL) (30 µL total clot volume). The pipette tip containing blood (25 µL) was first used to spread the clotting mixture droplet in a circular motion, after which the blood was then slowly released and subjected to the fluid cohesion effect to produce a circle (or halo-shaped appearance). The clots were then incubated at 37 °C for 1 h. Alongside the clots for sample treatment, positive and negative control wells were prepared. Positive control wells (representing 100% clot lysis) were prepared by mixing the assay buffer (75 µL) with blood (25 µL) (no clotting mixture present). Negative controls wells (representing 0% clot lysis) were prepared following the same method as that described above to produce halo-shaped clots however in the absence of a thrombolytic agent (i.e., only the assay buffer was added to the wells).

When incubation was complete, the clots were treated with their corresponding samples. A standard curve was produced using free uPA at concentrations of 5, 10, 20, and 40 nM. Alongside the standard curve, the different cubosome samples were added to the clots at the same concentration as that used in the in vitro plasminogen activation (S-2251) assay described above (1.6×10^{10} cubosomes mL^{-1}). For both the standard curve and cubosome samples, an aliquot (70 µL) of each sample was added to the clots. Once all samples were added to the clots, the plate was immediately placed into a FLUOstar Optima microplate reader (BMG Labtech) set to 37 °C and absorbance measurements were performed once every minute (10 flashes per read) for 3 h at 492 nm. No automated plate shaking was performed throughout the reaction. All uPA concentrations stated represent the final concentrations in the 100 µL reaction volume.

Immune Cell Association in Human Whole Blood: A human whole blood assay was conducted using a previously published method[41] with slight modifications. Fresh blood from healthy donors was collected into sodium heparin vacuette tubes (Greiner Bio-One) and aliquoted (100 µL) in polystyrene tubes (Falcon round-bottom polystyrene tubes, 5 mL) with informed participant consent in accordance with the University of Melbourne Human ethics approval 1443420 and the Australian National Health and Medical Research Council Statement on Ethical Conduct in Human Research. Cell numbers were counted using a CELL-DYN Emerald analyzer (Abbott). The cubosome samples were incubated with blood (100 µL) at 37 °C for 1 h at a particle-to-white blood cell ratio of 200:1. After incubation, the red blood cells were lysed using Pharm Lyse buffer (4 mL), followed by washing twice with flow cytometry staining (FACS) buffer (PBS containing 2 mM ethylenediaminetetraacetic acid and 0.5% w/v BSA) by centrifugation (500 *g*, 7 min). The remaining white blood cells were phenotyped at 4 °C for 1 h using an antibody cocktail consisting of CD66b BV421 (G10F5), CD45 V500 (H130), CD19 BV650 (HIB19), CD3 AF700 (SP34−2), CD14 APC-H7 (MΦP9), and CD56 PE (B159) in titrated concentrations. The cells were then washed twice with FACS buffer by centrifugation (500 *g*, 7 min), fixed by 1% w/v formaldehyde, and analyzed by flow cytometry (LSRFortessa, BD Biosciences). The data were analyzed using FlowJo V10.

In Vivo Biodistribution and Blood Clearance Studies: All in vivo studies were performed using C57BL/6J male mice aged 8–12 weeks (purchased from Monash University Animal Research Precinct, Victoria, Australia). All animal experiments were approved by the Alfred Research Alliance Animal Ethics Committee, Monash University (AEC number E/1625/2016/M). Mice were anesthetized with ketamine hydrochloride (100 mg kg^{-1}; Mavlab, Queensland, Australia) and xylazine hydrochloride (10 mg kg^{-1}; New South Wales, Australia) administered via intraperitoneal (IP) injection. When no longer responsive to toe pinch stimulation, the mice were intravenously administered, via tail vein injection, either free Cy7.5-labeled uPA or Cy7.5-labeled uPA encapsulated within the different cubosome nanocarriers. All mice were dosed with 0.175 µg per body weight (g) of total U-FRAG protein, for which the equivalent cubosome sample dose was 3×10^9 cubosomes g^{-1}.

Blood samples were then collected by clipping the mouse tail (no more than 2 mm from tail tip) and withdrawing an aliquot (2.5 µL) of blood using a pipette at the following time points post-injection: 2.5, 5, 10, 30, and 60 min. Immediately after each collection, the blood samples were transferred to a tube containing citrated PBS [97.5 µL; 3.2% sodium

citrate/PBS ratio = 1:9 (v/v)]. The blood samples were then stored at room temperature. After the final blood collection, the mice were euthanized by an overdose IP injection of ketamine/xylazine (300/30 mg/kg, respectively) and subjected to transcardial perfusion with PBS (20 mL) before the brain, liver, spleen, kidney, lung, heart, thigh (skeletal) muscle, and brain were harvested. The organs/tissue were briefly washed in chilled PBS before being dried of excess PBS and kept in a specimen container on ice. Both the blood and organ/tissue samples were shielded from light prior to fluorescence imaging.

For fluorescence imaging, the total volume (100 µL) of blood/citrated PBS samples was transferred to a 96-well plate with a clear base and black walls (Corning) and scanned on a near-infrared (NIR) Odyssey CLx scanner (LI-COR Biosciences, NE, USA) with fluorescence detected using the 800 nm line (scan channel intensity: 2, acquisition resolution: 42 µm, scanning focus offset: 4 mm). The organ/tissue samples were transferred directly onto the scanning plate of the NIR scanner with fluorescence detected using the 800 nm line (scan channel intensity: L2, acquisition resolution: 169 µm, scanning focus offset: 0.5 mm).

For the blood clearance analysis, the total fluorescence from each sample well was plotted against time using GraphPad Prism version 9.0 software (GraphPad Software, CA, USA) and the data points were fitted to a one-phase exponential decay nonlinear regression, which was used to calculate the half-life of each curve. For the biodistribution analysis, the mean fluorescence intensity was measured from a representative region within each organ/tissue sample (where the representative region was of identical shape and size for each measurement across all organs/tissues).

Statistical Analysis: All statistical analyses were performed using GraphPad Prism version 9.0 software (GraphPad Software). For size and ζ-potential of nanoparticles, data is shown as the mean ± SD (n = 3). For Figures 4–8, data is presented as the mean ± SEM (n = 3). Comparisons between three groups or more were performed by one-way ANOVA. For the ex vivo blood (halo) clot degradation assay, a paired analysis was performed between different groups (paired together for sharing identical blood donors in each assay), with Dunnett's post-hoc analysis comparing each cubosome sample to 10 nM free uPA. For the in vitro plasminogen activation (S-2251) assay, analysis was performed with Dunnett's post-hoc analysis (no matching or pairing) comparing each cubosome sample to 10 nM free uPA. For immune cell association, an unpaired analysis was performed with Dunnett's post-hoc test

comparing each cubosome sample to uPA@$^{+}$Cub. For the in vivo blood clearance and biodistribution analyses, an unpaired analysis was performed with Fisher's least significant difference post-hoc analysis. The blood clearance data points were fitted to a one-phase exponential decay nonlinear regression. A *p*-value of <0.05 was considered significant.

Minimum Information Reporting in Bio-Nano Experimental Literature (MIRIBEL): The studies conducted herein, including material characterization, biological characterization, and experimental details conform to the MIRIBEL reporting standard for bio-nano research,[44] and we include a companion checklist of these components in the supporting information.

Supporting Information

Supporting Information is available from the Wiley Online Library or from the author.

Acknowledgements

H.Y. and J.S.P. contributed equally to this work. We thank Dr. Chan-Jin Kim for operating EDX elemental mapping characterization. This research was funded and supported by a National Health and Medical Research Council (NHMRC) Project Grant (GNT1138361, C.E.H. and F.C.). F.C. and C.E.H. acknowledge the award of an NHMRC Senior Principal Research Fellowship (GNT1135806) and an NHMRC Research Fellowship (GNT1154270), respectively. J.S.P. acknowledges support from Australian Rotary Health, Rotary District 9830, and the Australian Government Research Training Program (RTP) Scholarship.

Conflict of Interest

The authors declare no conflict of interest.

Received: ((will be filled in by the editorial staff))
Revised: ((will be filled in by the editorial staff))
Published online: ((will be filled in by the editorial staff))

References

[1] S. Wang, X. Guo, W. Xiu, Y. Liu, L. Ren, H. Xiao, F. Yang, Y. Gao, C. Xu, L. Wang, *Sci. Adv.* **2020**, *6*, eaaz8204.

[2] S. Sharma, M. K. Masud, Y. V. Kaneti, P. Rewatkar, A. Koradia, M. S. A. Hossain, Y. Yamauchi, A. Popat, C. Salomon, *Small* **2021**, *17*, 2102220.

[3] C. Fong, T. Le, C. J. Drummond, *Chem. Soc. Rev.* **2012**, *41*, 1297.

[4] H. M. G. Barriga, M. N. Holme, M. M. Stevens, *Angew. Chem. Int. Ed.* **2019**, *58*, 2958.

[5] J. Zhai, C. Fong, N. Tran, C. J. Drummond, *ACS Nano* **2019**, *13*, 6178.

[6] Q. Xiao, Z. Wang, D. Williams, P. Leowanawat, M. Peterca, S. E. Sherman, S. Zhang, D. A. Hammer, P. A. Heiney, S. R. King, D. M. Markovitz, S. André, H.-J. Gabius, M. L. Klein, V. Percec, *ACS Cent. Sci.* **2016**, *2*, 943.

[7] L. Han, S. Che, *Adv. Mater.* **2018**, *30*, 1.

[8] A. E. Seago, P. Brady, J. P. Vigneron, T. D. Schultz, *J. R. Soc., Interface* **2009**, *6*, S165.

[9] V. Saranathan, C. O. Osuji, S. G. J. Mochrie, H. Noh, S. Narayanan, A. Sandy, E. R. Dufresne, R. O. Prum, *Proc. Natl. Acad. Sci. U. S. A.* **2010**, *107*, 11676.

[10] L. Van'T Hag, S. L. Gras, C. E. Conn, C. J. Drummond, *Chem. Soc. Rev.* **2017**, *46*, 2705.

[11] D. Demurtas, P. Guichard, I. Martiel, R. Mezzenga, C. Hébert, L. Sagalowicz, *Nat. Commun.* **2015**, *6*, 1.

[12] T. G. Meikle, S. Yao, A. Zabara, C. E. Conn, C. J. Drummond, F. Separovic, *Nanoscale* **2017**, *9*, 2471.

[13] C. Leal, N. F. Bouxsein, K. K. Ewert, C. R. Safinya, *J. Am. Chem. Soc.* **2010**, *132*, 16841.

[14] B. Angelov, A. Angelova, S. K. Filippov, M. Drechsler, P. Štěpánek, S. Lesieur, *ACS Nano* **2014**, *8*, 5216.

[15] J. A. Prange, S. Aleandri, M. Komisarski, A. Luciani, A. Käch, C.-D. Schuh, A. M. Hall, R. Mezzenga, O. Devuyst, E. M. Landau, *ACS Appl. Bio Mater.* **2019**, *2*, 2490.

[16] A. Angelova, B. Angelov, R. Mutafchieva, S. Lesieur, P. Couvreur, *Acc. Chem. Res.* **2011**, *44*, 147.

[17] C. V. Kulkarni, W. Wachter, G. Iglesias-Salto, S. Engelskirchen, S. Ahualli, *Phys. Chem. Chem. Phys.* **2011**, *13*, 3004.

[18] B. P. Dyett, H. Yu, J. Strachan, C. J. Drummond, C. E. Conn, *Nat. Commun.* **2019**, *10*, 4492.

[19] J. B. Strachan, B. P. Dyett, Z. Nasa, C. Valery, C. E. Conn, *J. Colloid Interface Sci.* **2020**, *576*, 241.

[20] B. P. Dyett, H. Yu, B. Lakic, N. De Silva, A. Dahdah, L. Bao, E. W. Blanch, C. J. Drummond, C. E. Conn, *J. Colloid Interface Sci.* **2021**, *600*, 14.

[21] M. J. Daley, M. S. Murthy, E. J. Peterson, *Ther. Adv. Drug Saf.* **2015**, *6*, 57.

[22] S. Schulman, R. J. Beyth, C. Kearon, M. N. Levine, *Chest* **2008**, *133*, 257S.

[23] R. Cheng, W. Huang, L. Huang, B. Yang, L. Mao, K. Jin, Q. ZhuGe, Y. Zhao, *ACS Nano* **2014**, *8*, 7746.

[24] M. T. Griffin, Y. Zhu, Z. Liu, C. K. Aidun, D. N. Ku, *Biomicrofluidics* **2018**, *12*, 042210.

[25] C. P. Molloy, Y. Yao, H. Kammoun, T. Bonnard, T. Hoefer, K. Alt, F. Tovar-Lopez, G. Rosengarten, P. A. Ramsland, A. D. van der Meer, A. van den Berg, A. J. Murphy, C. E. Hagemeyer, K. Peter, E. Westein, *J. Thromb. Haemost.* **2017**, *15*, 972.

[26] H. Yu, J. S. Palazzolo, J. Zhou, Y. Hu, B. Niego, S. Pan, Y. Ju, T.-Y. Y. Wang, Z. Lin, C. E. Hagemeyer, F. Caruso, *ACS Appl. Mater. Interfaces* **2022**, *14*, 3740.

[27] H. P. Ebben, M. V. van Burink, V. Jongkind, D. E. Mouwen, J. Udding, W. Wisselink, J. K. Kievit, A. M. Wiersema, K. Yeung, *Ann. Vasc. Surg.* **2018**, *48*, 111.

[28] H. Ejima, J. J. Richardson, K. Liang, J. P. Best, M. P. van Koeverden, G. K. Such, J. Cui, F. Caruso, *Science* **2013**, *341*, 154.

[29] Y. Ju, J. Cui, M. Müllner, T. Suma, M. Hu, F. Caruso, *Biomacromolecules* **2015**, *16*, 807.

[30] J. Zhou, Z. Lin, M. Penna, S. Pan, Y. Ju, S. Li, Y. Han, J. Chen, G. Lin, J. J. Richardson, I. Yarovsky, F, Caruso, *Nat. Commun.* **2020**, *11*, 4804.

[31] M. A. Rahim, S. L. Kristufek, S. Pan, J. J. Richardson, F. Caruso, *Angew. Chem. Int. Ed.* **2019**, *58*, 1904.

[32] A. Angelova, B. Angelov, B. Papahadjopoulos-Sternberg, M. Ollivon, C. Bourgaux, *Langmuir* **2005**, *21*, 4138.

[33] B. Angelov, A. Angelova, B. Papahadjopoulos-Sternberg, S. V. Hoffmann, V. Nicolas, S. Lesieur, *J. Phys. Chem. B* **2012**, *116*, 7676.

[34] A. Angelova, M. Ollivon, A. Campitelli, C. Bourgaux, *Langmuir* **2003**, *19*, 6928.

[35] A. Angelova, B. Angelov, B. Papahadjopoulos-Sternberg, M. Ollivon, C. Bourgaux, *J. Drug Delivery Sci. Technol*. **2005**, *15*, 108.

[36] J. Chen, S. Pan, J. Zhou, Q.-Z. Zhong, Y. Qu, J. J. Richardson, F. Caruso, *Chem. Mater*. **2020**, *32*, 6975.

[37] M. A. Rahim, K. Kempe, M. Müllner, H. Ejima, Y. Ju, M. P. van Koeverden, T. Suma, J. A. Braunger, M. G. Leeming, B. F. Abrahams, F. Caruso, *Chem. Mater.* **2015**, *27*, 5825.

[38] T. Bonnard, L. S. Law, Z. Tennant, C. E. Hagemeyer, *Sci. Rep.* **2017**, *7*, 2346.

[39] Y. Ju, H. G. Kelly, L. F. Dagley, A. Reynaldi, T. E. Schlub, S. K. Spall, C. A. Bell, J. Cui, A. J. Mitchell, Z. Lin, A. K. Wheatley, K. J. Thurecht, M. P. Davenport, A. I. Webb, F. Caruso, S. J. Kent, *ACS Nano* **2020**, *14*, 15723.

[40] S. Li, Y. Ju, J. Zhou, K. F. Noi, A. J. Mitchell, T. Zheng, S. J. Kent, C. J. H. Porter, F. Caruso, *ACS Appl. Mater. Interfaces* **2021**, *13*, 35494.

[41] J. Song, Y. Ju, T. H. Amarasena, Z. Lin, S. Mettu, J. Zhou, M. A. Rahim, C.-S. S. Ang, C. Cortez-Jugo, S. J. Kent, F. Caruso, *ACS Nano* **2021**, *15*, 10025.

[42] Y. Ju, J. Cui, H. Sun, M. Müllner, Y. Dai, J. Guo, N. Bertleff-Zieschang, T. Suma, J. J. Richardson, F. Caruso, *Biomacromolecules* **2016**, *17*, 2268.

[43] Y. Ju, C. Cortez-Jugo, J. Chen, T.-Y. Wang, A. J. Mitchell, E. Tsantikos, N. Bertleff-Zieschang, Y.-W. Lin, J. Song, Y. Cheng, S. Mettu, M. A. Rahim, S. Pan, G. Yun, M. L. Hibbs, L. Y. Yeo, C. E. Hagemeyer, F. Caruso, *Adv. Sci.* **2020**, *7*, 1902650.

[44] M. Faria, M. Björnmalm, K. J. Thurecht, S. J. Kent, R. G. Parton, M. Kavallaris, A. P. R. R. Johnston, J. J. Gooding, S. R. Corrie, B. J. Boyd, P. Thordarson, A. K. Whittaker, M. M. Stevens, C. A. Prestidge, C. J. H. Porter, W. J. Parak, T. P. Davis, E. J. Crampin, F. Caruso, *Nat. Nanotechnol.* **2018**, *13*, 777.

The synthesis of thrombolytic drug (uPA)-loaded lipid cubosomes coated with a low-fouling peptide incorporated within a metal–phenolic network and their application as nanocarriers of thrombolytic drugs are demonstrated. The metal–peptide–phenolic network-coated lipid cubosomes display low nonspecific uPA activity, reduced nonspecific cell association, prolonged circulating half-life, and reduced splenic uPA accumulation in mice.

H. Yu, J. S. Palazzolo, Y. Ju, B. Niego, S. Pan, C. E. Hagemeyer,* F. Caruso*

Polyphenol-Functionalized Cubosomes as Thrombolytic Drug Carriers